ACS APPLIED MATERIALS & INTERFACES

Research Article

www.acsami.org

Preparation of a Responsive Carbohydrate-Coated Biointerface Based on Graphene/Azido-Terminated Tetrathiafulvalene Nanohybrid Material

Izabela Kaminska,[†,‡] Alexandre Barras,[†] Yannick Coffinier,[†] Wojciech Lisowski,[‡] Saumya Roy,[∇] Joanna Niedziolka-Jonsson,[‡] Patrice Woisel,*[,§] Joel Lyskawa,[§] Marcin Opallo,[‡] Aloysius Siriwardena,[∇] Rabah Boukherroub,*[,†] and Sabine Szunerits*[,†]

[†]Institut de Recherche Interdisciplinaire (IRI), CNRS USR 3078, Université Lille 1, Parc de la Haute Borne, 50 avenue de Halley, BP 70478, 59658 Villeneuve d'Ascq, France

[‡]Institute of Physical Chemistry, Polish Academy of Sciences, Kasprzaka 44/52, 01-224 Warszawa, Poland

[§]USTL, Université Lille Nord de France Unité des Matériaux Et Transformations (UMET, UMR 8207), Equipe Ingénierie des Systèmes Polymères (ISP), F-59655 Villeneuve d'Ascq Cedex, France et ENSCL, F59655, Villeneuve d'Ascq, France

[∇]Laboratoire des Glucides (FRE3517), Université de Picardie Jules Vernes, 33 rue saint Leu, 80039 Amiens, France

ABSTRACT: A one-step method for the reduction of graphene oxide (GO) to reduced graphene oxide (rGO) is reported taking advantage of the electron-donor properties of an azido-terminated tetrathiafulvalene (TTF-N_3). The resulting graphene/TTF-N_3 nanohybrid material is characterized by X-ray photoelectron spectroscopy (XPS), Fourier transform infrared spectroscopy (FT-IR) spectroscopy, and by electrical and electrochemical means. The accessibility of the azide function to chemoselective modification by any alkyne-terminated partner molecule via Cu(I)-catalyzed "click" chemistry is demonstrated. In a proof of principle and motivated by the importance of glycan-modified materials, many alkynyl-terminated mannose units were grated onto graphene/TTF-N_3. The TTF-mannose units could be released efficiently from the graphene matrix by chemical oxidation of TTF-mannose surface units to TTF^{2+}-mannose, using $Fe(ClO_4)_3$ or the electron-deficient tetracationic cyclophane cyclobis(paraquat-*p*-phenylene) ($CBPQT^{4+}$).

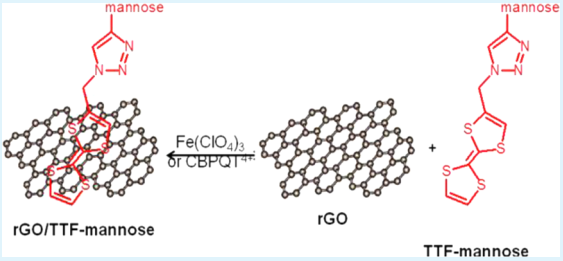

KEYWORDS: *graphene oxide, reduction, tetrathiafulvalene, click chemistry, host–guest chemistry, glycan switch*

1. INTRODUCTION

Graphene has attracted significant research interest, because of its remarkable electrical, thermal, and mechanical properties, which is a consequence of its two-dimensional hexagonal carbon lattice.[1] Because of its low cost of production, large specific surface area, and abundant surface chemistry, graphene has shown great promise in the development of novel composites, biosensors, and catalysts.[2] Different methods have been reported for the preparation of high-quality graphene, such as chemical vapor deposition (CVD) on metal or silicon substrates and mechanical exfoliation using strong oxidants.[3] The exfoliated sheets are distorted carbon networks carrying carbonyl, hydroxyl, and other oxygen-containing functional groups. Chemical reduction of graphene oxide (GO) using a reducing agent such as hydrazine is currently the most widely used approach for the removal of these oxygen groups and in the restoration of the sp^2 bonded carbon network.[4,5] However, agents such as hydrazine must be handled carefully, because of their toxic nature. The formation of graphene via chemical reduction in the presence of an organic reduction agent is an interesting alternative.[6−9] We[6,7] and other researchers[8,9] have shown that the formation of reduced GO can be achieved using aromatic organic molecules such as dopamine and tetrathiafulvalene (TTF). TTF and its derivatives are strong electron donors. The TTF unit, thanks to its multistable oxidation states (TTF^0, $TTF^{\bullet -}$, TTF^{2+}),[10] has been incorporated into electrochemically controllable supramolecular assemblies (e.g., rotaxanes, catenanes, pseudorotaxanes) with applications as logic gates, redox-controllable molecular machines or switches.[11−16] The use of TTF also allows modulation of the properties of graphene through its chemical modification in a noncovalent manner, taking advantage of strong $\pi-\pi$ interactions between the graphene sheets and the aromatic ring of TTF.[17,18] Motivated by the exceptional properties of TTF, we have recently reported on a one-step process for the simultaneous reduction of functionalization of GO using TTF.[7] Interest in the formed graphene/TTF nanocomposites is the possibility to release the noncovalent linked TTF molecules from the graphene matrix upon

Received: July 13, 2012
Accepted: September 12, 2012
Published: September 12, 2012

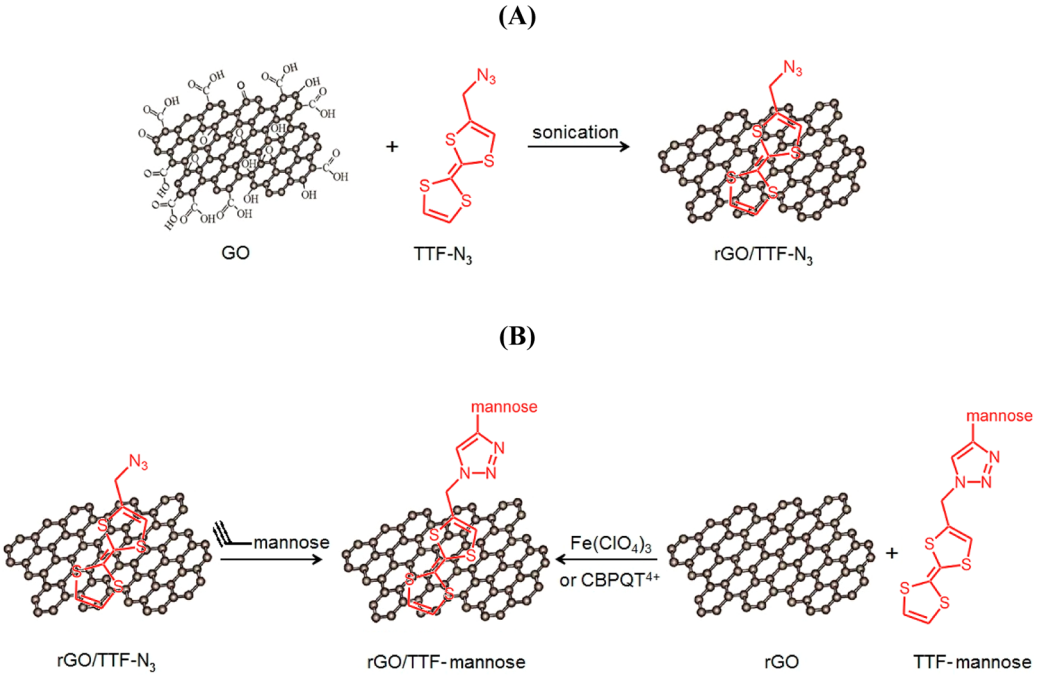

Figure 1. Schematic illustrations of (A) the formation of graphene/TTF-N_3 nanosheets and (B) Cu(I)-catalyzed "click" chemistry with alkynyl-mannose and the reversible release of TTF-mannose from a graphene matrix.

the chemical oxidation of TTF to TTF^{2+}, using an aqueous solution of $Fe(ClO_4)_3$.

We were curious to establish whether or not azide-terminated TTF (TTF-N_3) might behave similarly to TTF as it does toward GO. Since the electrochemical redox potential of the TTF-N_3/TTF-$N_3^{\bullet+}$ redox couple ($E^0 \approx 0.45$ V vs Ag/AgCl) is comparable to that of TTF,[7] azide-terminated TTF is expected to transfer electrons to GO, which reduces the potential by −0.7 V vs Ag/AgCl.[8,19] The formed graphene/TTF-N_3 nanocomposite material would subsequently be amenable to a Cu(I) catalyzed 1,3-dipolar cycloaddition strategy, thereby allowing the attachment of any alkyne-terminated molecule of choice to the graphene/TTF interface.[20−23] The concept of "click" chemistry, introduced by Sharpless and based on triazole ring formation between complementary azides and alkynes, is particularly well-suited for such a post-functionalization strategy, because of its compatibility with a wide range of functional groups coupled with its high reaction efficiency, its requirement of very mild reaction conditions, and its generality.[20,21,24] It will be demonstrated that graphene/TTF-N_3 nanocomposites can indeed be fabricated by simply mixing GO with TTF-N_3 at room temperature and sonication for 3 h (Figure 1A). In a proof of principle study it will be demonstrated that a 1,3-dipolar azide−alkyne cycloaddition strategy can effectively be applied to covalently graft alkynyl-mannose units onto the graphene/TTF-N_3 matrix (Figure 1B). The release of TTF-mannose units from the graphene network can be triggered either by chemical oxidation or by the formation of host−guest systems, as is the case with π-electron-deficient tetracationic cyclophane cyclobis(paraquat-*p*-phenylene) ($CBPQT^{4+}$) (see Figure 1B).[12,25]

2. EXPERIMENTAL SECTION

2.1. Materials. Graphite powder (particle size <20 μm), dimethylsulfoxide (DMSO), potassium chloride (KCl), CuI, triethylamine (TEA), ruthenium hexamine ($Ru(NH_3)_6$), tetrabutylammonium hexafluorophosphate ($TBAPF_6$), and tin-doped indium oxide coated glass (ITO) (sheet resistivity = 15−25 Ω cm^2) were purchased from Aldrich and used as-received.

Cyclophane cyclobis(paraquat-*p*-phenylene) ($CBPQT^{4+}$) was synthesized as reported previously.[26] The formation of α-propargyl mannopyranoside was achieved according to reports by Roy et al.[27] and Yeoh et al.[28] The azide-terminated tetrathiafulvalene (TTF-N_3) anchor was prepared from 2-(hydroxymethyl)tetrathiafulvalene, using a previously described protocol.[29]

2.2. Preparation of Graphene Oxide (GO). Graphene oxide (GO) was synthesized from graphite powder by a modified Hummers method.[30] Five milligrams (5 mg) of the synthesized GO was dispersed in 1 mL of water and exfoliated through ultrasonication for 3 h. This aqueous suspension of GO was used as a stock suspension in subsequent experiments.

2.3. Preparation of Graphene/Azide-Terminated Tetrathiafulvalene (rGO/TTF-N_3). The stock graphene oxide (GO) (5 mg/mL) suspension was diluted in water to obtain 0.5 mg/mL solution (1:10). TTF-N_3 (10 mM in DMF) was added to 1.5 mL of GO and the mixture was left for 3 h in an ultrasonic bath. The precipitate formed was separated from the aqueous supernatant by centrifugation at 14 000 rpm for 20 min. After washing with water (three times), the resulting precipitate was dried in an oven for several hours and then resuspended in DMF (2 mL) with the aid of ultrasonication for 30 min.

2.4. "Click" Reaction on rGO/TTF-N_3. rGO/TTF-N_3-modified ITO electrodes were prepared by casting 50 μL of graphene/TTF-N_3 solution in DMF onto a previously cleaned ITO substrate and heated at 70 °C. rGO/TTF-N_3 modified ITO surfaces were immersed into an aqueous solution (10 mL) of alkynyl-terminated mannose (2 mM), $CuSO_4 \cdot 5H_2O$ (200 μM), and L-ascorbic acid (300 μM), and the mixture was stirred at ambient temperature for 24 h. The resulting "clicked" graphene matrix was cleaned with EDTA (three times, 1 mM) to remove any remaining Cu(II) and finally with water (three times).

2.5. Determination of Coupling Efficiency of Glycans to rGO/TTF-N_3. A standard calibration curve was generated for determining carbohydrate concentrations by mixing aliquots of aqueous phenolic solution (5 wt %, 60 μL) and concentrated H_2SO_4 (900 μL) to a series of 60 μL aliquots of serially diluted aqueous

dx.doi.org/10.1021/am3013196 | ACS Appl. Mater. Interfaces 2012, 4, 5386−5393

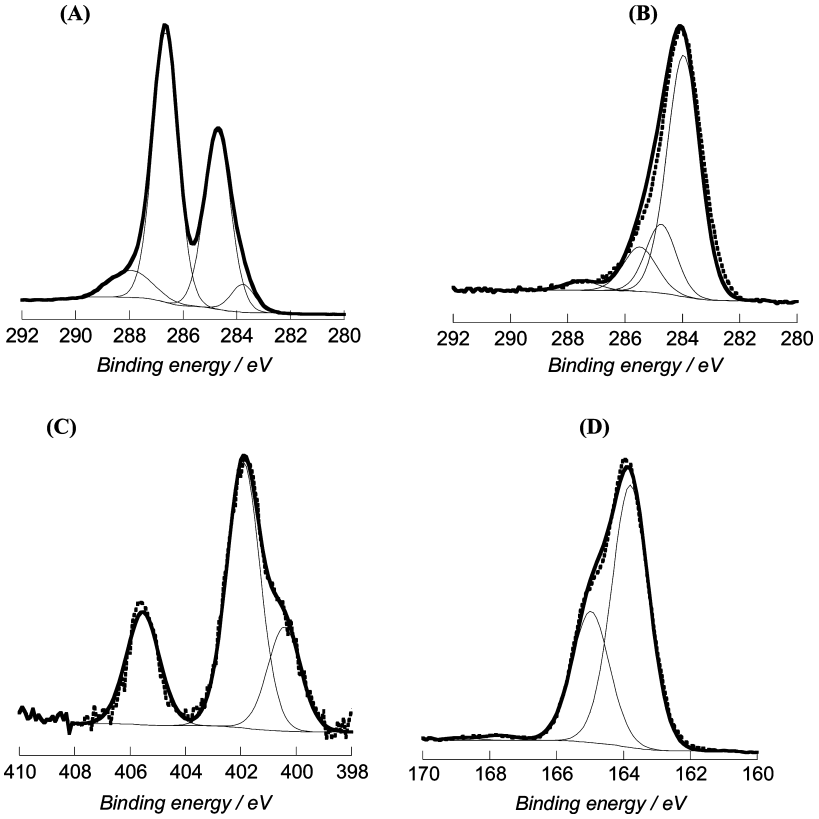

Figure 2. (A) C 1s spectrum of GO, (B) C 1s spectrum of GO after reaction with TTF-N_3, (C) N 1s spectrum of graphene/TTF-N_3, and (D) S 2p spectrum of graphene/TTF-N_3.

mannose solutions. Each was stirred for 10 min and then its absorption spectrum was recorded (Perkin−Elmer Lambda 950 dual beam system), using a phenol−H_2SO_4 mixture containing only 60 μL of water as a blank. The absorbance of the solution was measured at two wavelengths—λ_1 = 495 nm (absorption band of mannose complex) and λ_2 = 570 nm (background)—and the absorbance difference ($A_{495} - A_{570}$) was plotted against the concentration of the corresponding carbohydrate. To determine the coupling efficiency of mannose to graphene/TTF-N_3, the modified ITO interface was dipped for 60 min into 2 mL of the phenol/H_2SO_4 solution and the UV/vis spectrum was recorded.

2.6. Release of TTF-Mannose from rGO/TTF-Mannose Nanohybrid. ITO/rGO/TTF-mannose modified surfaces were prepared as described in section 2.4. Each surface was immersed into a vial filled with either 2 mM aqueous $Fe(ClO_4)_3$ solution (1 mL) or an aqueous $CBPQT^{4+}$ solution (2 mM or 100 μM). In order to examine the ability of the hybrid material to release TTF-mannose units as a function of time, the rGO/TFF-mannose matrix was immersed for exactly 1 min in either $Fe(ClO_4)_3$ or $CBPQT^{4+}$solutions. The resulting UV/vis spectrum was then recorded before the surface was reimmersed into either solution for 1 min. This sequence was repeated until no further change in the UV/vis spectrum was observed, suggesting that no further release of TTF-mannose residues could be triggered. In the case of release with $CBPQT^{4+}$, the increase of the absorption band at 855 nm due to the formation of the charge transfer complex of $CBPQT^{4+}$ with TTF was monitored, whereas, in the case of $Fe(ClO_4)_3$, the increase of the absorption band at 446 nm due to TTF was determined.

2.6. Characterization. *X-ray photoelectron Spectroscopy.* X-ray photoelectron spectroscopy (XPS) experiments were performed in a PHI 5000 VersaProbe - Scanning ESCA Microprobe (ULVAC-PHI, Japan/USA) instrument at a base pressure below 5 × 10^{-9} mbar. Monochromatic Al Kα radiation was used and the X-ray beam, focused to a diameter of 100 μm, was scanned on a 250 μm × 250 μm surface, at an operating power of 25 W (15 kV). Photoelectron survey spectra were acquired using a hemispherical analyzer at a pass energy of 117.4 eV with an energy step of 0.4 eV. Core-level spectra were acquired at a pass energy of 23.5 eV with a 0.1 eV energy step. All spectra were acquired with an angle of 90° between the X-ray source and the analyzer and with the use of low-energy electrons and low-energy Ar^+ ions for charge neutralization. After subtraction of the Shirley-type background, the core-level spectra were decomposed into their components with mixed Gaussian−Lorentzian (30:70) lineshapes, using the CasaXPS software. Quantification calculations were performed using sensitivity factors supplied by PHI.

FT-IR Spectroscopy. Fourier transform infrared (FT-IR) spectra in grazing-angle attenuated total reflectance (gATR mode) were recorded using a ThermoScientific FTIR instrument (Nicolet 8700) equipped with a VariGATR accessory (Harrick Scientific Products, Inc.). Spectra were collected at an incidence angle of 62.5° from normal with a resolution of 4 cm^{-1} by accumulating a minimum of 64 scans per sample. The rGO/TTF-N_3 was prepared by casting 50 μL of graphene/TTF composite materials on a cleaned glass substrate heated at 70 °C. The surface and the TTF-N_3 powder were placed on the center of the Ge crystal and a pressure was applied during measurements.

Cyclic Voltammetry. Cyclic voltammetry (CV) experiments were performed using an Autolab 20 potentiostat (Eco Chimie, Utrecht, The Netherlands). The electrochemical cell consisted of a working electrode (ITO or modified ITO), Ag/AgCl (Bioanalytical Systems, Inc.) as the reference electrode, and platinum wire as the counter electrode. CV measurements were performed in 5 mM $Ru(NH_3)_6$ in KCl (0.1 M) at a scan rate of ν = 0.1 V s^{-1}.

Graphene oxide (GO)- and rGO/TTF-N_3-modified ITO electrodes were prepared by casting 50 μL of an aqueous solution of either GO or rGO/TTF-N_3, respectively, onto the ITO substrate heated at 70 °C.

Conductivity Measurements. Electrical conductivity was determined via the Hall effect, using a the HL 5500 PC system in a standard four-probe setup. The graphene sample was prepared by filtration of the dispersion through a PVDF membrane filter.

UV/vis Measurements. Absorption spectra were recorded using a Perkin–Elmer Lambda UV/vis 950 spectrophotometer in plastic cuvettes with an optical path of 10 mm. The wavelength range was 400–1100 nm or 400–700 nm.

Atomic Force Microscopy. Atomic force microscopy (AFM) measurements were performed with a Dimension 3100 Model AFM (Veeco, Santa Barbara, CA) equipped with a Nanoscope IV controller (Digital Instruments) under ambient conditions (relative humidity = 30%, temperature = 22–24 °C). Rectangular single-beam silicon cantilevers (AFM-TM Arrow, Nanoworld) with spring constants of 42 N m^{-1} and typical resonant frequencies between 250 kHz and 300 kHz were used. All AFM images were acquired in the tapping mode at a constant force of 5–50 pN. A rGO/TTF-N_3 solution in DMF (10 μL) was deposited on a mica surface (Good Fellow) and dried at 70 °C for 3 h before AFM imaging.

3. RESULTS AND DISCUSSION

3.1. Formation of Reduced Graphene/TTF-N_3 Nanocomposite Material. We were interested in fabricating a rGO/TTF-N_3 nanohybrid in the knowledge that such a material should have potential application as a molecular switch. We have recently shown that a simple mixing of graphene oxide (GO) with TTF resulted in the reduction of GO to graphene (rGO) with simultaneous decorating rGO with TTF moieties.[7] Chemical oxidation of TTF to TTF^{2+} using an aqueous solution of $Fe(ClO_4)_3$ expelled the charged molecule from these functionalized graphene nanosheets, while subsequent immersion into neutral TTF solution allowed recapture of the TTF molecules. Motivated by the mild conditions typical of "click" chemistry, azide-terminated TTF (TTF-N_3) was investigated for its capability to reduce GO while simultanously incorporating itself into the graphene sheet. As was the case for unmodified TTF, the rGO/TTF-N_3 nanocomposite material is readily formed through the addition of TTF-N_3 to GO at room temperature, neutral pH, and under sonication. After 3 h of sonication, a precipitate formed that was soluble in DMF but nondispersible in water; this precipitate could be separated from the supernatant aqueous solution by centrifugation.

X-ray photoelectron spectroscopy (XPS) analysis was performed on GO before and after its reaction with TTF-N_3, to gain further information on its chemical composition. Chemically exfoliated GO contains a variety of functional groups, such as hydroxyl (C–OH), epoxide (C–O–C), carbonyl (C=O), and carboxyl (COOH) groups usually present at the defects and edges of the sheets. The C 1s core-level XPS spectrum of GO nanosheets is shown in Figure 2A and can be deconvoluted into four peak components with binding energies at ~283.8, 284.7, 286.7, and 287.9 eV, assigned to sp^2-hybridized carbon, C–H/C–C, C–O, and C=O species, respectively. The C/O ratio of GO is 1.73, which is comparable to reported data in the literature.[31,32] After reaction of GO with TTF-N_3, XPS analysis of the resulting precipitate indicates significant changes in the C 1s core-level spectrum (Figure 2B). The intensity of the sp^2-hybridized carbon at 283.8 eV became dominant. Additional bands at 284.9, 285.6, and 287.5 eV are also observed and can be attributed to C–H/C–C, C–S, and C=O/C=S species functions, respectively. The ratio of carbon to oxygen is increased to ~10. This value is comparable to that reported by Stankovich et al. for hydrazine-reduced GO with C/O = 10.3 (from ref 4) and is three times larger than that observed for photochemically oxidized GO with C/O = 3.3.[32] The presence of TTF-N_3 in the graphene matrix is further confirmed by the appearance of two bands in the XPS spectrum, at 164 and 400 eV, which are attributable to N 1s and S 2p, respectively (see Figures 2C and 2D).

The N 1s core level spectrum (Figure 2C) shows contributions at 405.5 eV, assigned to the central electron-deficient nitrogen (N=N=N) of the azide, and at 401.8 eV, which are due to the two lateral N atoms of the azide (N=N=N) with a ratio of 1:2, in accordance with the presence of an azido group.[33] An additional band at 400.4 eV corresponds to one N atom of the amide function formed most likely by partial decomposition of the azide function upon X-ray exposure during XPS analysis.[34] Figure 2D shows the S 2p spectrum of the nanocomposites material. Because of the spin–orbital splitting effect, the S 2p spectrum can be composed of S $2p_{3/2}$ (163.8 eV) and S $2p_{1/2}$ (164.9 eV) peaks separated by 1.1 eV, with an intensity ratio of 2:1. The small contribution at 167.7 eV corresponds to higher oxidation states of C=S.[35] The results are comparable to those obtained when GO is treated with unmodified TTF. The data confirm that the influence of the N_3-functional group seems to be negligible.

The success of the incorporating of TTF-N_3 units into the reduced graphene nanosheets was additionally confirmed by FTIR spectroscopy (Figure 3). The FTIR spectrum of rGO/TTF-N_3 shows a strong band at ~2100 cm^{-1}, which is ascribed to the asymmetric azide group stretching mode, as in the case of TTF-N_3.[36] In addition, the observed bands at 3070, 1650, 1228, 1099, and 875–790 cm^{-1} can be assigned to C–H, C=C, C–N, C=S, and C–H/N–H stretching modes, respectively. Significantly, no band at 3250 cm^{-1} is present, suggesting a high degree of reduction of GO.

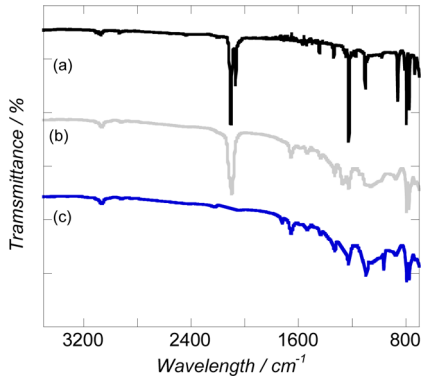

Figure 3. FTIR spectra of TTF-N_3 (black spectrum), rGO/TTF-N_3 (gray spectrum), and rGO/TTF-mannose (blue spectrum).

3.2. Electrical and Electrochemical Behavior of rGO/TTF-N_3 Composite Interfaces. Electrochemical measurements were performed to characterize the electrical properties of rGO/TTF-N_3 composite material. Figure 4A shows cyclic voltammetry (CV) scans of a bare ITO electrode before and after its drop casting with a film of either GO or rGO/TTF-N_3 in $Ru(NH_3)_6^{3+/2+}$. As reported previously, the drop-casting process is very reproducible and leads to homogeneous distributions of GO and rGO/TTF-N_3 flakes on the ITO interface.[6,7] For the sake of comparison, the CV data of graphene obtained through hydrazine reduction of GO is shown. The results indicate that the detected cathodic current density of rGO/TTF-N_3 exceeds that of a bare ITO electrode, while GO-modified ITO interfaces exhibit an almost insulating character. The data indicate that the rGO/TTF-N_3 films are endowed with a unique electronic structure and enhanced

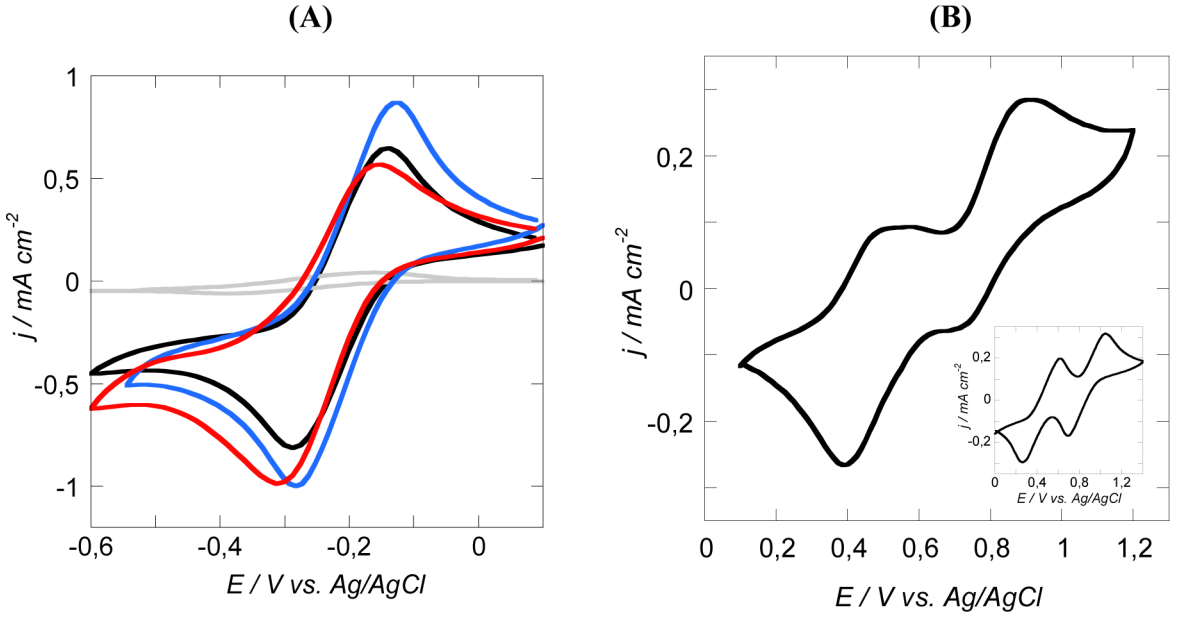

Figure 4. Cyclic voltammetry (CV) scans (voltammograms) of ITO compounds: (A) bare ITO (black trace), ITO/GO (gray trace), ITO/graphene (reduced using hydrazine) (blue trace), and ITO/graphene/TTF-N_3 (red trace) (for each, the solution was 5 mM $Ru(NH_3)_6^{3+}$ in a 0.1 M KCl aqueous solution), and (B) ITO/graphene/TTF-N_3 in a TBAPF_6/acetonitrile solution. Inset in panel B shows the CV voltammogram of TTF-N_3 (1 mM) in acetonitrile recorded on ITO. Scan rate = 0.1 V s^{-1}.

electron transfer capabilities, compared to those of a bare ITO electrode. The electron transfer rate on graphene sheets formed by hydrazine reduction of GO is somewhat faster than those observed for the rGO/TTF-N_3 interface.

The room-temperature conductivity of the formed rGO/TTF-N_3 composite material also measured, using a standard four-probe method. The nanocomposites showed a conductivity of 0.3 S m^{-1}, which is lower than that obtained for hydrazine-reduced graphene (145 S m^{-1}) using the same approach. However, this value is comparable to those reported recently by Zhang and co-workers, where GO was reduced to graphene in the presence of metal ions and TTF.[8]

The good conductivity of the film enables the electrochemical detection of TTF-N_3 moieties in the graphene matrix (Figure 4B). Two redox waves, with E_1^0 = 0.45 V and E_2^0 = 0.81 V (vs Ag/AgCl), are seen, which are characteristic of TTF oxidation in a one-electron process to $TTF^{\bullet +}$, followed by a further oxidation to TTF^{2+}.[10] The first wave is rather broad, because of the possible presence of π-dimers, resulting from a coupling of two TTF radical cations.[37] These potentials are ~0.35 V more anodic than that observed for the rGO/TTF interface. However, the potential is comparable to that recorded for a 1 mM solution of TTF-N_3 in acetonitrile recorded on an ITO electrode (see inset in Figure 4B). The second redox wave is shifted to more-negative values, compared to solutions of TTF-N_3, and is most likely due to donor−acceptor interactions between the graphene and TTF-N_3 moieties. The loading of TTF-N_3 on the rGO surface was calculated by integrating the anodic peak area according to

$$\Gamma = \frac{Q_A}{nFA}$$

where F is the Faraday constant, n the number of electrons exchanged (here, n = 1), and A the surface area (here, A = 0.2 cm^2). A value of $\Gamma_{azide} = (3.40 \pm 0.8) \times 10^{15}$ molecules cm^{-2} is obtained, which is four times larger than that obtained in the case of rGO/TTF.[7]

3.3. "Clicking" of Alkynyl-Mannose to Graphene/TTF-N_3. The reactivity of the azide function in the graphene/TTF-N_3 composite was used for linking alkynyl-terminated mannose in a "click chemistry" approach, using the copper(I)-catalyzed Huisgen 1,3-dipolar cycloaddition (see Figure 1). The change of the N 1s XPs spectrum upon the "click" reaction of alkynyl-terminated mannose to graphene/TTF-N_3 is consistent with the conversion of the $-N_3$ group to the −NH− function (see Figure 5). The disappearance of the band at 405.23 eV

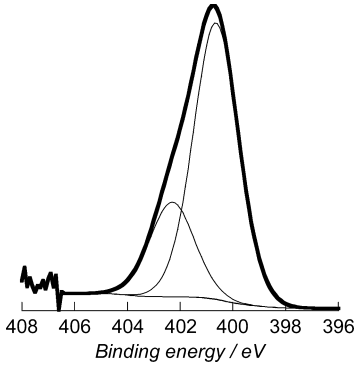

Figure 5. N 1s high-resolution XPS spectrum of graphene/TTF-N_3 after reaction with alkynyl-mannose.

indicates the conversion of the azide group. The high-resolution N 1s spectrum shows a broad signal centered at 400.7 eV, which was fitted and deconvoluted into two peaks, at 402.9 eV (N−N═N) and 400.6 eV (N−N═N) with the ratio of the peak areas being ~1:2.5 (the theoretical value should be 1:2).[38] The lower peak area ratio between the bands at 402.9 and 400.6 eV might be indicative that some NH_2 functions, being part of the band at 400.6 eV, are present. In addition, the coupling of alkynyl-terminated mannose was spectroscopically

dx.doi.org/10.1021/am3013196 | ACS Appl. Mater. Interfaces 2012, 4, 5386−5393

confirmed by the disappearance of the characteristic azide vibration at 2100 cm^{-1} and the appearance of bands at 1100 cm^{-1} (triazole breathing mode) at 965 cm^{-1} (C−N stretching mode) (see spectrum c in Figure 3).[39]

The loading of mannose "clicked" onto the to rGO/TTF-N_3 nanocomposite interfaces was estimated using a colorimetric assay, based on the specific reaction of carbohydrates with phenol in concentrated sulfuric acid.[40,41] The method allowed the amount of sugar to be estimated as $\Gamma_{mannose} = (2.2 \pm 0.5) \times 10^{15}$ molecules cm^{-2}. This indicates that ~64% of the surface-linked azide groups ($\Gamma_{azide} = (3.40 \pm 0.8) \times 10^{15}$ molecules cm^{-2}) got converted to triazole rings. This result is in accordance with the XPS analysis (Figure 5), which indicates the formation of NH_2 groups in addition to triazole rings, thus decreasing the amount of "clicked" mannose.

3.4. Chemically Triggered Release of Mannose from the Graphene Matrix. One of the main interests in the developed graphene-based composite material is the possibility to chemically trigger the release of TTF-glycans as well as to reintegrate TTF-glycans into the graphene matrix. This would allow, for the first time, accessibility to a reusable glycansensor for the detection of glycan−protein interactions at hand. Indeed, establishing the details of specific carbohydrate−protein interactions is an essential part in developing a clear understanding of the roles of surface carbohydrates in biology and, moreover, how their often intrinsically low affinity associations with proteins are transformed into those of biological significance.[42]

Two methods of triggering the controlled release of TTF-mannose from the graphene/TTF-mannose were used. Upon treatment with an aqueous solution of $Fe(ClO_4)_3$, $(1.2 \pm 0.5) \times 10^{15}$ molecules cm^{-2} are expelled from the graphene surface, corresponding to 65% of total TTF-mannose release (see Figure 6A).[7]

The release efficiency was compared to that observed upon the addition of $CBPQT^{4+}$ to graphene/TTF mannose hybrid (see Figure 6A). TTF has proven to be a versatile redox-active system for the construction of switchable host−guest and interlocked systems.[13] In particular, pseudo-rotaxanes prepared from electron-rich TTF units and the electron-deficient $CBPQT^{4+}$ unit have emerged as important systems for the construction of redox tunable assemblies.[43,44] The π-electron-deficient tetracationic cyclophane cyclobis(paraquat-*p*-phenylene) ($CBPQT^{4+}$) moiety is known to be able to form strong charge-transfer complexes with TTF derivatives in aqueous media.[14,45] It is thus likely that $CBPQT^{4+}$ "pulls" the TTF-mannose units from the graphene matrix, as schematically illustrated in the inset of Figure 6B. The release of TTF-mannose from the graphene matrix into solution by $CBPQT^{4+}$ can be conveniently assessed by detecting the formation of a TTF-$CBPQT^{4+}$ host−guest complex at $\lambda \approx 855$ nm (see Figure 6C).[25,44] Treatment of the hybrid nanomaterial with 2 mM $CBPQT^{4+}$ did induce the release of TTF-mannose units. As depicted in Figure 6A, the initial release kinetics of the TTF-mannose is much faster when rGO/TTF-mannose is exposed to $CBPQT^{4+}$ and the release efficiency reaches 100% after exposure for 1 h.

AFM imaging provided an estimate of the thickness of the rGO/TTF-mannose nanocomposite before and after the triggered release of TTF-mannose from it. Figure 7A shows an AFM image of a rGO/TTF-mannose film formed by depositing 10 μL of a solution in rGO/TTF-mannose on mica and drying at 70 °C for 3 h. A section analysis allows a

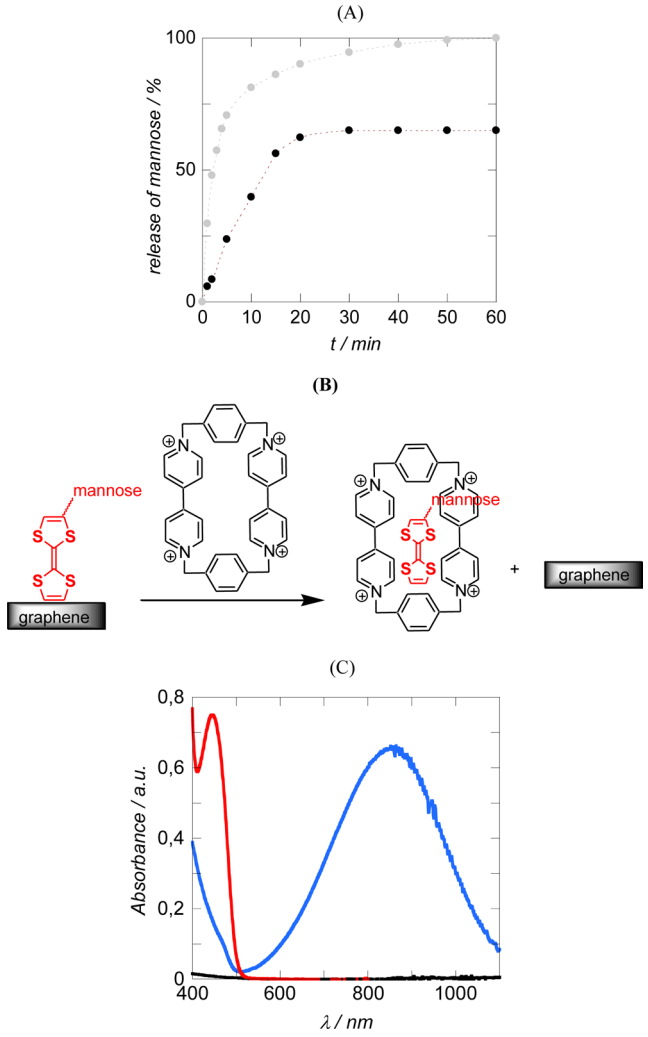

Figure 6. (A) Time-dependent release of TTF-mannose from rGO/TTF-mannose composite deposited on ITO using 2 mM $CBPQT^{4+}$ (gray circles) and 2 mM $Fe(ClO_4)_3$ (black circles) determined by the increase in the absorbance band at 855 nm (see Figure 6C) of the TTF/$CBPQT^{4+}$ complex, and $Fe(ClO_4)_3$ (2 mM (♦) determined by the absorbance band at 446 nm. (B) Schematic scheme of the release of TTF-mannose with the addition of $CBPQT^{4+}$. (C) UV/vis spectrum of TTF-N_3 (red spectrum), $CBPQT^{4+}$ (black spectrum), and TTF-N_3/$CBPQT^{4+}$ charge-transfer complex (blue spectrum).

thickness of 1.02 nm with a root-mean-square (rms) value of 0.31 nm to be determined. This value is typical of a functional-molecule-modified single-layer graphene.[6] In an additional experiment, the hybrid nanointerface was immersed for 60 min into an aqueous solution of 2 mM $CBPQT^{4+}$, then washed with water and dried as done previously. An AFM scan of the resulting interface (Figure 7B) showed its thickness to have decreased to a value of 0.57 nm with a rms value of 0.37 nm. An identical value was obtained upon the oxidation of TTF-mannose in solution and then transferring it onto mica. Immersing a rGO, where the TTF-mannose had been released into a fresh solution of TTF-mannose for 20 min, gave an AFM scan corresponding to a film thickness of ~1 nm and is consistent with the reintegration of functional TTF-mannose units into the graphene network. This reintegration was also confirmed by the presence of the electrochemical signature of TTF (by cyclic voltammetry) and a value of $\Gamma_{mannose} = (1.8 \pm 0.5) \times 10^{15}$ molecules cm^{-2} could be estimated. This is

dx.doi.org/10.1021/am3013196 | ACS Appl. Mater. Interfaces 2012, 4, 5386−5393

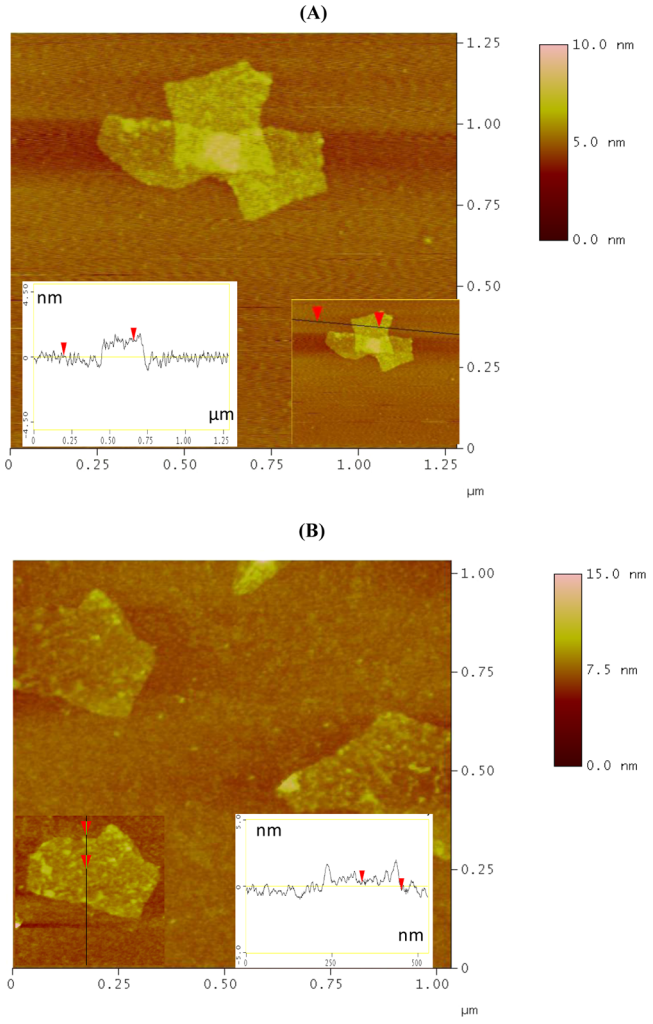

Figure 7. AFM images of graphene/TTF-mannose film (A) before and (B) after immersion of 60 min into a 2 mM solution of $CBPQT^{4+}$.

comparable to the initial value of $\Gamma_{mannose} = (2.2 \pm 0.5) \times 10^{15}$ molecules cm^{-2} and indicates the highly reversible nature of the process.

4. CONCLUSION

In conclusion, a new approach to reduced and chemically modified graphene oxide is demonstrated using TTF-N_3 as an electron donor and surface functionalization molecule. X-ray photoelectron spectroscopy (XPS) and Fourier transform infrared (FT-IR) spectroscopic data confirm the formation of the novel hybrid material. The azide-functional groups borne by the TTF moieties can be readily reacted with alkynyl-terminated molecules in a "click" chemistry approach, using the copper(I)-catalyzed Huisgen 1,3-dipolar cycloaddition. We were particularly interested in pursuing the development of a carbohydrate-coated biointerface, which would allow selective capture of lectins from unfractionated protein mixtures. Therefore, in a proof of principle, alkynyl-terminated mannose was linked to the graphene nanocomposite material. The TTF-mannose could be released either by the oxidation of TTF, using $Fe(ClO_4)_3$, or by the formation of host–guest complexes. Although, here, the formation of a colored charge-transfer complex between TTF and $CBPQT^{4+}$ has been used to spectroscopically follow the release of TTF from the graphene matrix, other molecules such as cyclodextrins might be considered in the future. Further interest of such a "switchable" glycan interface involves the possibility to control the multivalency effect, which is of high importance in glycan/protein (such as a bacteria, lectin or antibody) interactions. Diassembly of TTF-mannose units from the graphene matrix, as is possible in the nanobiointerface fabricated here, would be expected to lead to the collapse of the carbohydrate coating. This, in turn, would result in the disruption of any multivalent carbohydrate–protein interaction that had been established and, as a consequence, the desorption of the surface-adhered protein from the graphene matrix. Work toward such applications will be reported in due course.

AUTHOR INFORMATION

Corresponding Author

*E-mail: Sabine.Szunerits@iri.univ-lille1.fr, sabine.szunerits@gmail.com.

Notes

The authors declare no competing financial interest.

ACKNOWLEDGMENTS

I.K. thanks the International PhD Projects Programme of the Foundation for Polish Science, cofinanced from European Regional Development Fund within Innovative Economy Operational Programme "Grants for Innovation". The Centre National de la Recherche Scientifique (CNRS), and the Nord-Pas de Calais Région are gratefully acknowledged for financial support. A.S. thanks the CEFIPRA for a postdoctoral fellowship to S.R. and financial support.

REFERENCES

(1) Geim, A. K.; Novoselov, K. S. *Nat. Mater.* **2007**, *6*, 183–191.
(2) Dreyer, D. R.; Park, S. J.; Bielawski, C. W.; Ruoff, R. S. *Chem. Soc. Rev.* **2010**, *39*, 228–240.
(3) Rao, C. N. R.; Sood, A. K.; Subrahmanyam, K. S.; Govindaraj, A. *Angew. Chem. Inter. Ed.* **2009**, *48*, 7752–7777.
(4) Stankovich, S.; Dikin, D. A.; Piner, R. D.; Kohlhaas, K. A.; Kleinhammes, A.; Jia, Y.; Wu, Y.; Nguyen, S. T.; Ruoff, R. S. *Carbon* **2007**, *45*, 1558–1565.
(5) Tung, V. C.; Allen, M. J.; Yang, Y.; Kaner, R. B. *Nat. Nanotechnol.* **2009**, *4*, 25–29.
(6) Kaminska, I.; Das, M. R.; Coffinier, Y.; Niedziolka-Jonsson, J.; Sobczak, J.; Woisel, P.; Lyskawa, J.; Opallo, M.; Boukherroub, R.; Szunerits, S. *ACS Appl. Mater. Interfaces* **2012**, *4*, 1016–1020.
(7) Kaminska, I.; Das, M. R.; Coffinier, Y.; Niedziolka-Jonsson, J.; Woisel, P.; Opallo, M.; Szunerits, S.; Boukherroub, R. *Chem. Commun.* **2012**, *48*, 1221–1223.
(8) Yang, G.; Zhang, G.; Sheng, P.; Sun, F.; Wu, W.; Zhang, D. *J. Mater. Chem.* **2012**, *22*, 4391–4395.
(9) Xu, L. Q.; Yang, W. J.; Neoh, K.-G.; Kang, E.-T.; Fu, G. D. *Macromolecules* **2010**, *43*, 8336–8339.
(10) Canevet, D.; Salle, M.; Zhang, G. P.; Zhang, D.; Zhu, D. *Chem. Commun.* **2009**, *7*, 2245–2269.
(11) Yamada, J.; Sugimoto, T. In *TTF Chemistry. Fundamentals and Applications of Tetrathiafulvalene*; Springer–Verlag: Heidelberg, Germany, 2004.
(12) Guo, X.; Zhou, Y.; Feng, M.; Xu, Y. X.; Zhang, D.; Gao, H.; Fan, Q.; Zhu, D. *Adv. Funct. Mater.* **2007**, *17*, 763–769.
(13) Klajn, R.; Fang, L.; Coskun, A.; Olson, M. A.; Wesson, P. J.; Stoddart, J. F.; Grzybowski, B. A. *J. Am. Chem. Soc.* **2009**, *131*, 4233–4235.
(14) Bigot, J.; Charleux, B.; Cooke, G.; Delattre, F.; Fournier, D.; Lyskawa, J.; Sambe, L.; Stoffelbach, F.; Woisel, P. *J. Am. Chem. Soc.* **2010**, *132*, 10796–10801.

(15) Bigot, J.; Charleux, B.; Cooke, G.; Delattre, F.; Fournier, D.; Lyskawa, J.; Stoffelbach, F.; Woisel, P. *Macromolecules* **2010**, *43*, 82−90.
(16) Yasuda, T.; Tanabe, K.; Tsuji, T.; Coti, K. K.; Aprahmian, I.; Stoddart, J. F.; Kato, T. *Chem. Commun.* **2010**, *16*, 1224−1226.
(17) Ghosh, A.; Rao, K. V.; Voggu, R.; George, S. J. *Chem. Phys. Lett.* **2010**, *488*, 198−201.
(18) Varhese, N.; Ghosh, A.; Voggu, R.; Gosh, S.; Rao, C. N. R. *J. Phys. Chem. C* **2009**, *113*, 16855−16859.
(19) Shao, Y.; Wang, J.; Engelhard, M.; Wang, C.; Lin, Y. *J. Mater. Chem.* **2010**, *20*, 743−748.
(20) Jin, Z.; McNicjolas, T. P.; Shih, C.-J.; Wang, Q. H.; Paulus, G. L. C.; Hilmer, A. J.; Shimizu, S.; Strano, M. S. *Chem. Mater.* **2011**, *23*, 3362−3370.
(21) Wang, H.-X.; Zhou, K.-G.; Xie, Y.-L.; Zeng, J.; Chai, N.-N.; Li, J.; Zhang, H.-L. *Chem. Commun.* **2011**, *47*, 5747−5749.
(22) Devadoss, A.; Chidsey, C. E. D. *J. Am. Chem. Soc.* **2007**, *129*, 5370−5371.
(23) Pan, Y.; Bao, H.; Sahoo, N. G.; Wu, T.; Li, L. *Adv. Funct. Mater.* **2011**, *21*, 2754−5763.
(24) Kolb, H. C.; Finn, M. G.; Sharpless, K. B. *Ang. Chem. Int. Ed.* **2001**, *40*, 2004−2021.
(25) Barka-Bouaifel, F.; Niedziolka-Jonsson, J.; Castel, X.; Saison, O.; Akjouj, A.; Pennec, Y.; Djafari-Rouhani, B.; Woisel, P.; Lyskawa, J.; Samba, L.; G., C.; Bezzi, N.; Boukherroub, R.; Szunerits, S. *J. Mater. Chem.* **2011**, *21*, 3006−3013.
(26) Asakawa, M.; Dehaen, W.; L'abbe, G.; Menzer, S.; Nouwen, J.; Raymo, F. M.; F., S. J.; Williams, D. J. *J. Org. Chem.* **1996**, *61*, 9591−9595.
(27) Roy, B.; Mukhopadhyay, B. *Tetahedron Lett.* **2007**, *48*, 3783−3787.
(28) Yeoh, K. K.; Butters, T. D.; Wilkinson, B. L.; Fairbanks, A. J. *Carbohydr. Res.* **2009**, *344*, 586−591.
(29) Garin, J.; Orduna, J.; Uriel, S.; Moore, A. J.; Bryce, M. R.; Wegener, S.; Yufil, D. S.; Howard, J. A. K. *Synthesis* **1994**, *5*, 489−493.
(30) Das, M. R.; Sarma, R. K.; Saikia, R.; Kale, V. S.; Shelke, M. V.; Sengupta, P. *Colloid Surf. B* **2011**, *83*, 16−22.
(31) Lia, K.-H.; Mittal, A.; Bose, S.; Leighton, C.; Myhoyan, K. A.; Macosko, C. W. *ACS Nano* **2011**, *5*, 1253−1258.
(32) Fellahi, O.; Das, M. R.; Coffinier, Y.; Szunerits, S.; Hadjersi, T.; Maamache, M.; Boukherroub, R. *Nanoscale* **2011**, *3*, 4662−4669.
(33) Chidsey, C. E. D. *Langmuir* **2006**, *22*, 2457−2464.
(34) Liu, L.-H.; Zorn, G.; Castner, D. G.; Solanki, R.; Lernerd, M. M.; Yan, M. *J. Mater. Chem.* **2010**, *20*, 5041−5046.
(35) Choudhury, D.; Das, B. D.; Sarma, D. D.; Rao, C. N. R. *Chem. Phys. Lett.* **2010**, *497*, 66−69.
(36) Barras, A.; Szunerits, S.; Marcon, L.; Monfilliette-Dupont, N.; Boukherroub, R. *Langmuir* **2010**, *26*, 13168−13172.
(37) Lyskawa, J.; Sallé, M.; Balandier, J.-Y.; Le Derf, F.; Levillain, E.; Allain, M.; Viel, P.; Palacin, S. *Chem. Commun.* **2006**, 2233−2235.
(38) Qin, G.; Santos, C.; Zhang, W.; Li, Y.; Kumar, A.; Erasquin, U. J.; Liu, K.; Muradov, P. *J. Am. Chem. Soc.* **2010**, *132*, 16432−16441.
(39) Hannant, J.; Hedley, J. H.; Pate, J.; Walli, A.; Al-Said, S. A. F.; Galindo, M.; Connolly, B. A.; Horrocks, B. R.; Houlton, A.; Pike, A. R. *Chem. Commun.* **2010**, *46*, 5870−5872.
(40) Wang, X.; Ramstrom, O.; Yan, M. *J. Mater. Chem.* **2009**, *19*, 8944−8949.
(41) Durka, M.; Buffet, K.; Iehl, J.; Holler, M.; Nierengarten, J.-F.; Taganna, J.; Bouckaert, J.; Vincent, S. P. *Chem. Commun.* **2011**, *47* (4), 1321−1323.
(42) Mammen, M.; Choi, S.-K.; Whitesides, G. M. *Angew. Chem., Int. Ed.* **1998**, *37*, 2755−2794.
(43) Spruell, J. M.; Paxton, W. F.; Olsen, J.-C.; Benitez, D.; Tkatchouk, E.; Stern, C. L.; Trabolsi, A.; Friedman, D. C.; Goddard, W. A.; Stoddart, J. F. *J. Am. Chem. Soc.* **2009**, *131*, 11571−11580.
(44) Cooke, G.; Garety, J. F.; Hewage, S. G.; Rabani, G.; Rotello, V. M.; Woisel, P. *Chem. Commun.* **2006**, 4119.
(45) Sambe, L.; Stoffelbach, F.; Lyskawa, J.; Delattre, F.; Fournier, D.; Bouteiller, L.; Charleux, B.; Cooke, G.; Woisel, P. *Macromolecules* **2011**, *44*, 6532−6538.